AD-A111 790 VIRGINIA POLYTECHNIC INST AND STATE UNIV BLACKSBURG --ETC F/G 20/4
COMPUTATION OF THREE-DIMENSIONAL VISCOUS FLOW OVER BLUNT LIFTIN--ETC(U)
MAY 81 K Y SZEMA, C H LEWIS

UNCLASSIFIED NL

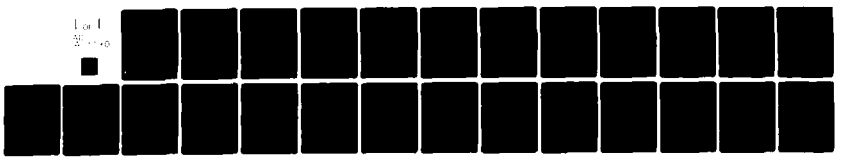

END
DATE FILMED
4-82
DTIC

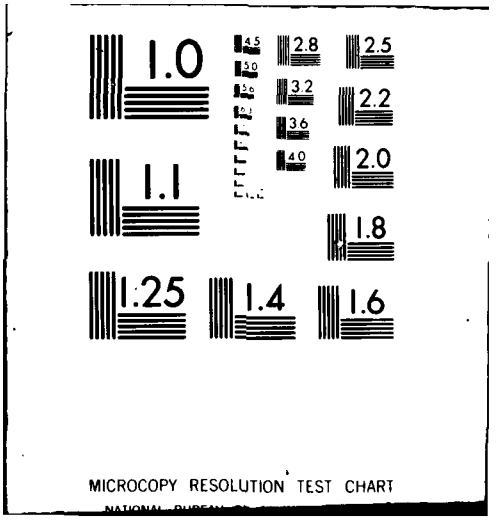
1.0
1.1
1.25
1.4
1.6
1.8
2.0
2.2
2.5
2.8
3.2
3.6
4.0
4.5
5.0
MICROCOPY RESOLUTION TEST CHART

(2)

COMPUTATION OF THREE-DIMENSIONAL VISCOUS FLOW OVER BLUNT LIFTING BODIES AT HIGH ANGLE OF ATTACK

K. Y. Szema* and C. H. Lewis**

Virginia Polytechnic Institute and State University
Aerospace and Ocean Engineering Department
Blacksburg, Virginia

14 MAY 81

ABSTRACT

The viscous shock-layer equations for three-dimensional hypersonic flows of a perfect gas or equilibrium air over lifting bodies at high angles of attack have been developed. For the complex three-dimensional reentry vehicle geometries of interest, the resulting equations are written in a nonorthogonal, body-oriented coordinate system, and the three velocity components are defined in the nonorthogonal coordinate directions. Since the viscous shock-layer governing equations are parabolic in both the streamwise and crossflow directions, the equations are solved by a highly efficient finite-difference scheme. The principal advantages of this technique are (i) the numerical method can be used to predict the flowfield about arbitrary geometries in both subsonic and supersonic regions, (ii) the solution is direct, and (iii) the effects of inviscid-viscous interactions are uniformly valid throughout the shock layer. Numerical solutions have been obtained for a 1:1.4 (perfect gas), 1:2 ellipsoid in a perfect gas or equilibrium air and the nose portion of the shuttle orbiter at zero, 10 and 25-deg angles of attack. Comparisons were made with inviscid solutions and existing experimental data, and the agreement is good for all the cases.

INTRODUCTION

Various analyses are available to investigate the flowfields and wall-measurable quantities for hypersonic flow past an axisymmetric blunt body at different angles of attack. However, the effects of the noncircular body geometry can be significant, and the main purpose of this study is to develop a technique to predict hypersonic viscous flows over a noncircular body at typical planetary entry conditions.

Recently a numerical method for 3-D laminar, transitional and/or turbulent hypersonic flows of perfect gas over a blunt body, used for planetary probes, has been investigated[1] at different angles of attack by using an

*Research Associate
**Professor

implicit finite-difference viscous shock-layer analysis. However, that analysis is valid for axisymmetric bodies only. For the complex three-dimensional lifting reentry vehicle geometries of interest, the resulting equations are written in a nonorthogonal body-oriented coordinate system, and the three velocity components are defined in the nonorthogonal coordinate directions. This procedure is different from writing the equations in an orthogonal coordinate system and explicitly performing a coordinate transformation. Since the viscous shock-layer equations are parabolic in both the streamwise and crossflow directions, the equations were solved by a highly efficient finite-difference scheme[1,2]. The principle advantages of this technique are (i) the numerical method can be used to predict the flowfield about arbitrary geometries in both subsonic and supersonic regions, (ii) the solution is direct, and (iii) the effects of inviscid-viscous interactions are included within a single set of governing equations which are uniformly valid throughout the shock layer.

The basic formulation of the problem is presented in Section 2. Boundary conditions at the body surface and immediately behind the shock are given in Section 3. Coordinates and method of solution are presented in Sections 4 and 5, respectively. The results are discussed in Section 6, and the conclusions are presented in Section 7.

BASIC FORMULATION

The basic equations are derived from the steady Navier-Stokes equations in general body-oriented tensor form (Figure 1). One of the coordinates, $\xi 1$, is chosen in the general axial direction, and another, $\xi 2$, in a direction normal to the body, and the third, $\xi 3$, around the body. The coordinate system requires orthognality only at the body surface. The normal velocity v and normal coordinate $\xi 2$ are assumed to be of order ϵ, and all terms which are of higher order than ϵ are neglected. The methods of obtaining these equations are discussed in detail elsewhere[2,3]. The nondimensional form of the viscous shock-layer equations that are applicable in the present case can be written as follows:

Continuity Equation:

$$\frac{\partial}{\partial \xi_1}\left(\rho u g^{1/2}\right) + \frac{\partial}{\partial \xi_2}\left(\rho v g^{1/2}\right) + \frac{\partial}{\partial \xi_3}\left(\rho w g^{1/2}\right) = 0 \tag{1}$$

ξ_1-Momentum:

$$\rho u \frac{\partial u}{\partial \xi_1} + \rho v \frac{\partial u}{\partial \xi_2} + \rho w \frac{\partial}{\partial \xi_3} + \rho \left[u^2 \left\{ \begin{matrix} 1 \\ 1\ 1 \end{matrix} \right\} + 2uv \left\{ \begin{matrix} 1 \\ 1\ 2 \end{matrix} \right\} \right.$$

$$\left. + 2uw \left\{ \begin{matrix} 1 \\ 1\ 3 \end{matrix} \right\} + v^2 \left\{ \begin{matrix} 1 \\ 2\ 2 \end{matrix} \right\} + 2vw \left\{ \begin{matrix} 1 \\ 2\ 3 \end{matrix} \right\} + w^2 \left\{ \begin{matrix} 1 \\ 3\ 3 \end{matrix} \right\} \right]$$

$$+ \frac{g_{22}}{g} \left[g_{33} \frac{\partial P}{\partial \xi_1} - g_{13} \frac{\partial P}{\partial \xi_3} \right]$$

$$= \varepsilon^2 \left[\frac{1}{g_{22}} \left(\frac{\partial \mu}{\partial \xi_2} \frac{\partial u}{\partial \xi_2} + \mu \frac{\partial^2 u}{\partial \xi_2^2} \right) \right] \tag{2}$$

ξ_2-Momentum:

$$\rho u \frac{\partial v}{\partial \xi_1} + \rho v \frac{\partial v}{\partial \xi_2} + \rho w \frac{\partial v}{\partial \xi_3} + \rho \left[u^2 \left\{ {2 \atop 1\,1} \right\} + 2uv \left\{ {2 \atop 1\,2} \right\} \right.$$

$$\left. + 2uw \left\{ {2 \atop 1\,3} \right\} + v^2 \left\{ {2 \atop 2\,2} \right\} + 2vw \left\{ {2 \atop 2\,3} \right\} + w^2 \left\{ {2 \atop 3\,3} \right\} \right]$$

$$+ \frac{1}{g_{22}} \frac{\partial P}{\partial \xi_2} = 0 \tag{3}$$

ξ_3-Momentum:

$$\rho u \frac{\partial w}{\partial \xi_1} + \rho v \frac{\partial w}{\partial \xi_2} + \delta w \frac{\partial w}{\partial \xi_3} + \rho \left[u^2 \left\{ {3 \atop 1\,1} \right\} + 2uv \left\{ {3 \atop 1\,2} \right\} + 2uw \left\{ {3 \atop 1\,3} \right\} \right.$$

$$\left. + v^2 \left\{ {3 \atop 2\,2} \right\} + 2vw \left\{ {3 \atop 2\,3} \right\} + w^2 \left\{ {3 \atop 3\,3} \right\} \right] + \frac{g_{22}}{g} \left[g_{11} \frac{\partial P}{\partial \xi_3} \right.$$

$$\left. - g_{13} \frac{\partial P}{\partial \xi_1} \right] = \varepsilon^2 \left[\frac{1}{g_{22}} \left(\frac{\partial \mu}{\partial \xi_2} \frac{\partial w}{\partial \xi_2} + \mu \frac{\partial^2 w}{\partial \xi_2^2} \right) \right] \tag{4}$$

Energy Equation:

$$\rho u \frac{\partial h}{\partial \xi_1} + \rho v \frac{\partial h}{\partial \xi_2} + \rho w \frac{\partial h}{\partial \xi_3} - \left[u \frac{\partial P}{\partial \xi_1} + v \frac{\partial P}{\partial \xi_2} \right.$$

$$\left. + w \frac{\partial P}{\partial \xi_3} \right] = \varepsilon^2 \left[\frac{1}{g_{22}} \left(\frac{\partial}{\partial \xi_2} \left(\frac{\mu}{Pr} \right) \frac{\partial h}{\partial \xi_2} + \frac{\mu}{Pr} \frac{\partial^2 h}{\partial \xi_2^2} \right) \right]$$

$$+ \varepsilon^2 \left\{ \mu \left[\frac{g_{11}}{g_{22}} \left(\frac{\partial u}{\partial \xi_2} \right)^2 + 2 \frac{g_{13}}{g_{22}} \frac{\partial u}{\partial \xi_2} \frac{\partial w}{\partial \xi_2} + \frac{g_{33}}{g_{22}} \left(\frac{\partial w}{\partial \xi_2} \right)^2 \right] \right\} \tag{5}$$

It should be noted that the Prandtl number is assumed constant for a perfect gas and is a function of pressure and temperature for a gas in chemical equilibrium.

Equation of State

$$\rho = \rho(p, h) \tag{6}$$

For a perfect gas, Equation (6) has the analytical form

$$\rho = \gamma p/[(\gamma-1)RT]$$

where γ is the ratio of specific heats. For the chemical equilibrium assumption, the functional relation may be given by a table or an approximate analytical expression (curve fits) which are given in detail in Reference 4.

In the governing equations $\left\{ \begin{matrix} i \\ j\ k \end{matrix} \right\}$ are Christoffel symbols of the second kind, and the matrix g_{ij} can be obtained numerically from the grid generation procedure.

BOUNDARY CONDITION

In order to solve the above set of governing equations, it is essential to specify appropriate boundary conditions at the body surface and at the shock. At the body surface (wall), no-slip and no-temperature-jump conditions were used. Consequently, $u_w = v_w = w_w = 0$, and the wall temperature or heat-transfer rate was specified. The conditions immediately behind the shock were obtained by using the Rankine-Hugoniot relations. However, before those equations may be applied, the tangential and normal components of the velocity must be found. These components are obtained by the method of Rakich[5]. An orthogonal set of vectors with $\vec{N}$ a unit vector normal to the shock surface and $\vec{T}$ a tangent vector is considered. The N-T plane is parallel to the direction of freestream $\vec{U}_\infty$. Then the two-dimensional Rankine-Hugoniot relations are used to calculate the conditions behind the shock. The total velocity can be written as

$$\vec{U} = U_T \vec{T} + U_N \vec{N}$$

$$= \left[U_T \left(\frac{U_z - bN_z}{a} \right) - U_N \left(\frac{\sin\sigma}{c} \right) \right] \hat{e}_z$$

$$+ \left[U_T \left(\frac{U_r - bN_r}{a} \right) + U_N \left(\frac{\cos\sigma}{c} \right) \right] \hat{e}_r$$

$$+ \left[U_T \left(\frac{U_\phi - bN_\phi}{a} \right) - U_N \left(\frac{\cos\sigma \, \mathrm{Tan}\delta}{c} \right) \right] \hat{e}_\phi \tag{7}$$

where a, b, c, σ and δ are given by Rakich[5]. After the velocity behind the shock has been calculated, it is necessary to rotate these components into a body-normal nonorthogonal coordinate system. This is done by expressing the vectors $\hat{e}_z$, $\hat{e}_r$, $\hat{e}_\phi$ in terms of $\vec{g}_1$, $\vec{g}_2$, $\vec{g}_3$ in the ξ_1, ξ_2, ξ_3 directions

$$\begin{bmatrix} \hat{e}_z \\ \hat{e}_r \\ \hat{e}_\phi \end{bmatrix} = \begin{bmatrix} \frac{\partial z}{\partial \xi_1} & \frac{\partial r}{\partial \xi_1} & r\frac{\partial \phi}{\partial \xi_1} \\ \frac{\partial z}{\partial \xi_2} & \frac{\partial r}{\partial \xi_2} & r\frac{\partial \phi}{\partial \xi_2} \\ \frac{\partial z}{\partial \xi_3} & \frac{\partial r}{\partial \xi_3} & r\frac{\partial \phi}{\partial \xi_3} \end{bmatrix}^{-1} \begin{bmatrix} \vec{g}_1 \\ \vec{g}_2 \\ \vec{g}_3 \end{bmatrix} \tag{8}$$

Using Equation 8, the shock velocity components in the body-normal nonorthogonal coordinate system are determined.

COORDINATE GENERATION

Based on the general curvilinear coordinate governing equations, a body-oriented nonorthogonal coordinate system is constructed. This is first done on the surface of the body, where $\xi_2 = 0$, and then extended to the points away from the surface of the body. The coordinate system requires orthogonality only at the body surface, and the ξ_2 coordinate is always orthogonal to ξ_1 and ξ_3. The approach used is an extension of that presented by Blottner[6] and a detailed discussion of a similar procedure can be found in Reference 3.

METHOD OF SOLUTION

Davis[7] presented an implicit finite-difference method to solve the viscous shock-layer equations for axially symmetric flows. Murray and Lewis[2] extended the method of solution to three-dimensional high angle of attack conditions. The present method of solution is identical to that of Murray and Lewis. Therefore, only an overview of the solution procedure is presented.

The solution begins on the blunt nose by obtaining an approximate stagnation solution in the wind-fixed coordinate system. The 3-D solution begins on the windward plane and marches around the body obtaining a converged solution in each ϕ sweep. After completing a sweep in the ϕ direction, the procedure then steps downstream in ξ_1 and begins the next ϕ sweep. At each point the equations are solved in the following order (i) ϕ-momentum, (ii) energy, (iii) ξ_1-momentum, (iv) integration of continuity for Y_s, and (v) coupled continuity and normal momentum equations.

RESULTS AND DISCUSSION

Numerical solutions of the three-dimensional nonorthogonal shock-layer equations were obtained for a 1:1.4, 1:2 ellipsoid and the nose portion of

the shuttle orbiter at different angles of attack. It should be mentioned here that the wind-fixed coordinate system is used in the 1:2 ellipsoid 10-deg angle of attack case. The freestream conditions for these cases are given in Table 1. Comparisons are made for shock standoff distance, surface pressure distribution and heat-transfer rate with inviscid results and existing experimental data.

Shock-standoff distance as a function of the coordinate along the body surface in different ϕ-planes is illustrated in Figures 2 and 3. The inviscid solutions from Marconi and Yaeger[8] are also presented and are in very good agreement with the present nonorthogonal viscous shock-layer calculations. It is noted that the shock standoff distance increases more rapidly between ϕ = 0 and 30-deg for the 1:2 ellipsoid case than for the 1:1.4 case. However, this would be expected because the body curvature in the transverse direction is smaller for the 1:2 ellipsoid case in this region.

Figures 4 and 5 present the surface pressure distribution along the body at different ϕ-planes for these two cases. Some inviscid pressure results are also presented. It is noted that the inviscid data are in very good agreement with present results.

Figures 6 and 7 show the convective heating rate in several ϕ-planes along the body surface. The solution for Case 1 is compared with the experimental data given by Hillsamer and Rhudy[9]. The results show that the present prediction is in excellent agreement with the experimental data. Because of the streamwise body curvature effects, the heating rate is higher at ϕ = 90 and 30-deg than ϕ = 0 deg near the stagnation region for the 1:2 ellipsoid case. Except in the stagnation region, as was expected, the convective heat-transfer rate decreases with increasing ϕ.

Figures 8, 9 and 10 present the modified 1:2 ellipsoid geometry, surface pressure and convective heating rate for an equilibrium air calculation. As shown in Figure 9, the surface pressure is in reasonably good agreement with the inviscid solution. Since the geometry near the stagnation region is very flat and narrow, the convective heating rate decreased rapidly between ϕ = 0 and 30-deg. After ϕ = 30 deg, a much smaller heating rate change is noticed in Figure 10.

Figures 11 to 16 are the body geometry and results of the space shuttle orbiter nose portion up to seven nose radii. The cross section and longitudinal slope of the shuttle orbiter are given in Figure 11. It is noted that on the windward side, the body is relatively flat and the transverse direction curvature changes rapidly at about ϕ = 65-deg. The shock standoff distance in different ϕ-planes along the body is shown in Figure 12. Because of the flat windward side, the shock standoff distance decreased slightly on the windward side and then increased rapidly on the leeward side. The inviscid results are also presented, and the agreement is very good. Figure 13 presents the surface pressure distribution around the body at the s = 5.32 station. A very small pressure change was detected on the windward side ($\phi \leq 50^{o}$). However, a rapidly decreasing surface pressure was noticed in the region $50 < \phi < 90$ due to the transverse curvature effect. On the leeward side ($\phi > 90^{o}$), the pressure tends to stabilize and the change is small once again. Figure 14 shows that the same trend is followed for all stations along the body surface. Finally, the temperature profiles normal to the body

surface at s = 0 (stagnation point) and s = 5.325 and the convective heating rate along the body surface are plotted in Figures 15 and 16. Since no other data are available for this case, only the present results are presented here. For the same reason discussed earlier, the temperature and heating rate jump in the region $60 < \phi < 90$ was also noticed.

CONCLUSIONS

The main objective of this study is to investigate the influence of the noncircular body on the shock-layer flow phenomena within reasonable computing times. A general nonorthogonal shock-layer analysis is used. The present surface pressure, shock standoff distance and convective heating rate predictions are in good agreement with inviscid solutions and existing experimental data. The viscous shock-layer technique requires much less computing time than the time-dependent method[10] (Table 1). In the future we plan to include the transitional and/or turbulent flow in the technique.

LIST OF SYMBOLS

C_p^* specific heat at constant pressure

$\hat{e}_i$ unit vector of a general orthogonal coordinate system

$\vec{g}_1, \vec{g}_2, \vec{g}_3$ vectors in ξ_1 (streamwise), ξ_2 (normal) and ξ_3 (circumferential) directions

g_{ij} metrics $g_{ij} = \frac{\partial z}{\partial \xi_i}\frac{\partial z}{\partial \xi_j} + \frac{\partial r}{\partial \xi_i}\frac{\partial r}{\partial \xi_j} + r^2 \frac{\partial \phi}{\partial \xi_i}\frac{\partial \phi}{\partial \xi_j}$

g $\det(g_{ij}) = g_{11}\, g_{22}\, g_{33} - g_{22}\, g_{13}^2$

h static enthalpy, h^*/U_∞^{*2}

$\vec{N}$ shock-normal vector

p pressure

Pr Prandtl number

R_n body nose radius

T temperature

T_{ref}^* reference temperature, U_∞^{*2}/C_p^*

$\vec{T}$ shock-tangent vector

u, v, w streamwise, normal and crossflow velocity components nondimensionalized by the freestream velocity U_∞^*

U_N velocity component normal to the shock

U_T velocity component tangent to the shock

z,r,ϕ cylindrical coordinates

Y_s shock standoff distance

α angle of attack

γ ratio of specific heats

ε Reynolds number parameter $\varepsilon^2 = \mu^*_{ref}/\rho^*_\infty U^*_\infty R^*_n$

μ viscosity, μ^*/μ^*_{ref}

μ_{ref} reference viscosity, $\mu^*(T_{ref})$

ξ_1,ξ_2,ξ_3 computational coordinates

ρ density, ρ^*/ρ^*_∞

$\left\{ \begin{matrix} i \\ j\ k \end{matrix} \right\}$ Christoffel symbol of the 2nd kind, $\frac{1}{2}\sum_m g^{im}\left[\frac{\partial g_{mk}}{\partial \xi_j} + \frac{\partial g_{mj}}{\partial \xi_k} - \frac{\partial g_{jk}}{\partial \xi_m}\right]$

Subscript

∞ dimensional freestream conditions

Superscript

$*$ dimensional quantity

REFERENCES

1. Szema, K. Y. and Lewis, C. H.: "Three-Dimensional Hypersonic Laminar, Transitional and/or Turbulent Shock Layer Flow." AIAA Paper No. 80-1457, July 1980.

2. Murray, A. L. and Lewis, C. H.: "Hypersonic Three-Dimensional Viscous Shock-Layer Flow over Blunt Bodies," AIAA J., Vol. 16, No. 12, pp. 1279-1286, December 1978.

3. Helliwell, W. S., Dickinson, R. P. and Lubard, S. C.: "Viscous Flow over Arbitrary Geometries at High Angle of Attack." AIAA Paper No. 80-0064, January 1980.

4. Thareja, R. R., Szema, K. Y. and Lewis, C. H.: "Three-Dimensional Viscous Shock-Layer Analysis of Laminar and/or Turbulent Flows in Chemical Equilibrium," 12th Navy Symposium on Aeroballistics, DTNSRDC, Maryland, May 1981.

5. Rakich, J. V.: "A Method of Characteristics for Steady 3-D Supersonic Flow with Application to Inclined Bodies of Revolution." NASA TN D-5341, October 1969.

6. Blottner, F. G. and Ellis, M.: "Three-Dimensional Incompressible Boundary Layer on Blunt Bodies." Sandia Laboratories, SLA-73-0366, April 1973.

7. Davis, R. T.: "Numerical Solution of the Hypersonic Viscous Shock Layer Equations." AIAA J., Vol. 8, No. 5, pp. 843-851, May 1970.

8. Marconi, F. and Yaeger, L.: "Development of a Computer Code for Calculating the Steady Super/Hypersonic Inviscid Flow Around Real Configurations." NASA CR-2675, April 1976.

9. Hillsamer, M. E. and Rhudy, J. P.: "Heat Transfer and Shadowgraph Tests of Several Elliptical Lifting Bodies at Mach 10," AEDC-TDR-64, February 1964, AD429931.

10. Kutler, P., Pedelty, J. A. and Pulliam, T. H.: "Supersonic Flow over Three Dimensional Ablated Nosetips Using an Unsteady Implicit Numerical Procedure. AIAA Paper No. 80-0063, January 1980.

TABLE 1. Test Case Conditions

Case	1	2	3	4
Body Geometry	1:1.4 (ellipsoid)	1:2 (ellipsoid)	1:2 (modified ellipsoid)	Shuttle
T_∞ (^oR)	81.5	203.5	540.0	94.87
ρ_∞, slug/ft^3	4.118E-6	2.340E-4	7.99E-4	1.0528E-3
P_∞, psia	0.041	0.567	5.145	0.0119
T_w (^oR)	470	366	3139	540
Re_∞ (1/ft)	2.38E+6	4.993E+6	3.3058E+7	5.5696E+5
α, deg	0^o	10^o	0^o	25^o
Gas Model	perfect gas	perfect gas	equilibrium air	perfect gas
Computational Time*(Min) IBM 370/3032	6	12	16	12

*It takes approximately two hours CDC 7600 time for a sphere nose when using time dependent method of Reference 10.

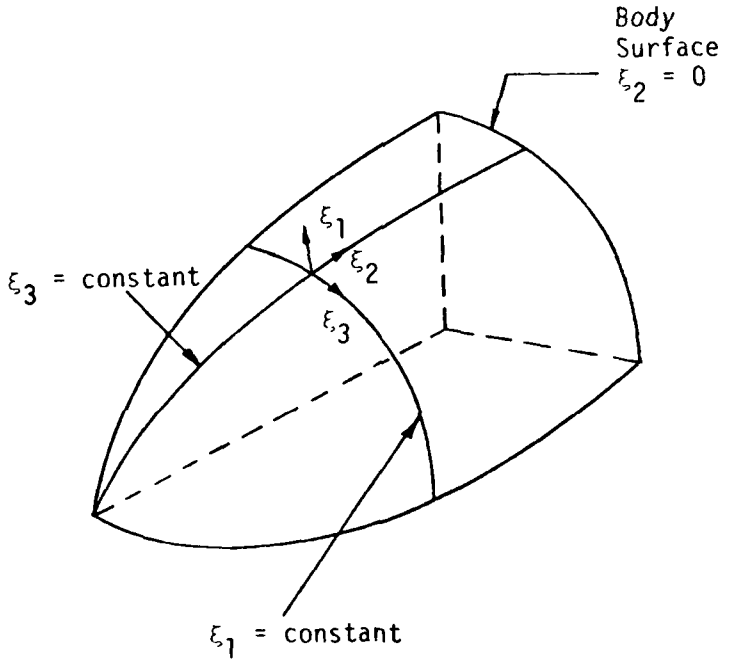

Figure 1. Coordinate System

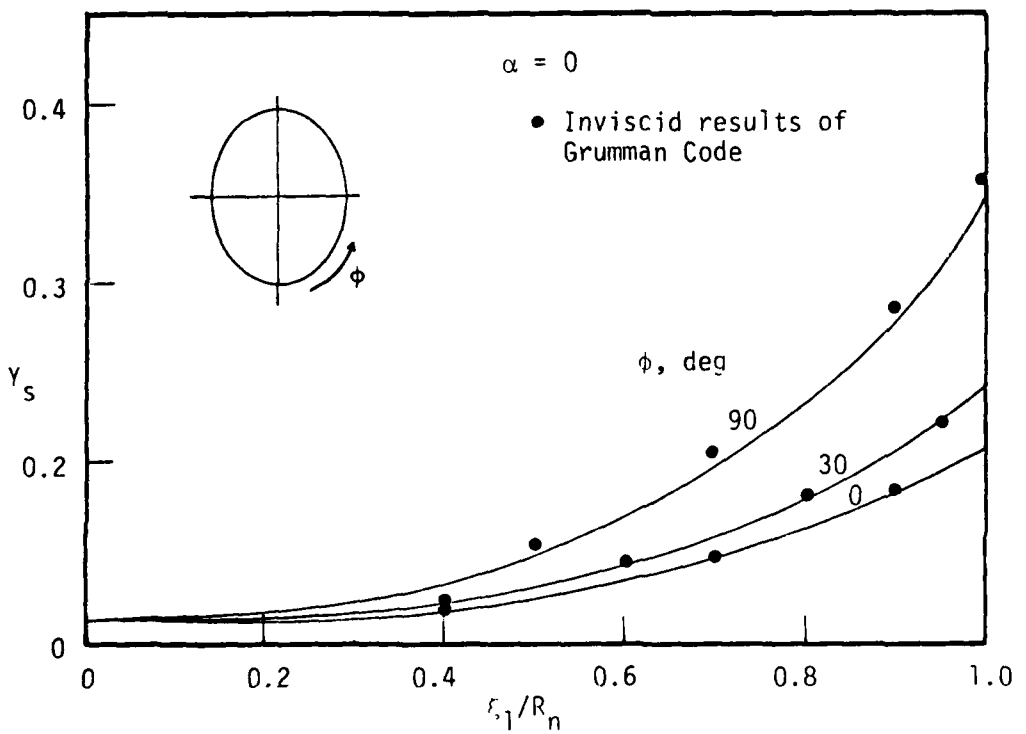

Figure 2. Shock Standoff Distance of 1:1.4 Ellipsoid

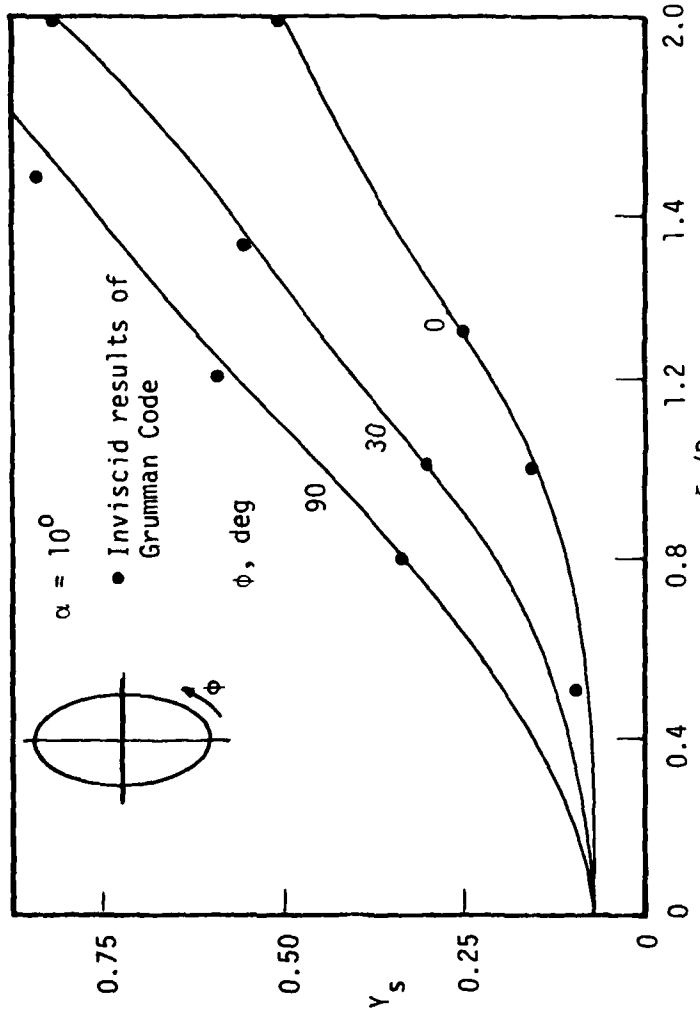

Figure 3. Shock Standoff Distance for 1:2 Ellipsoid

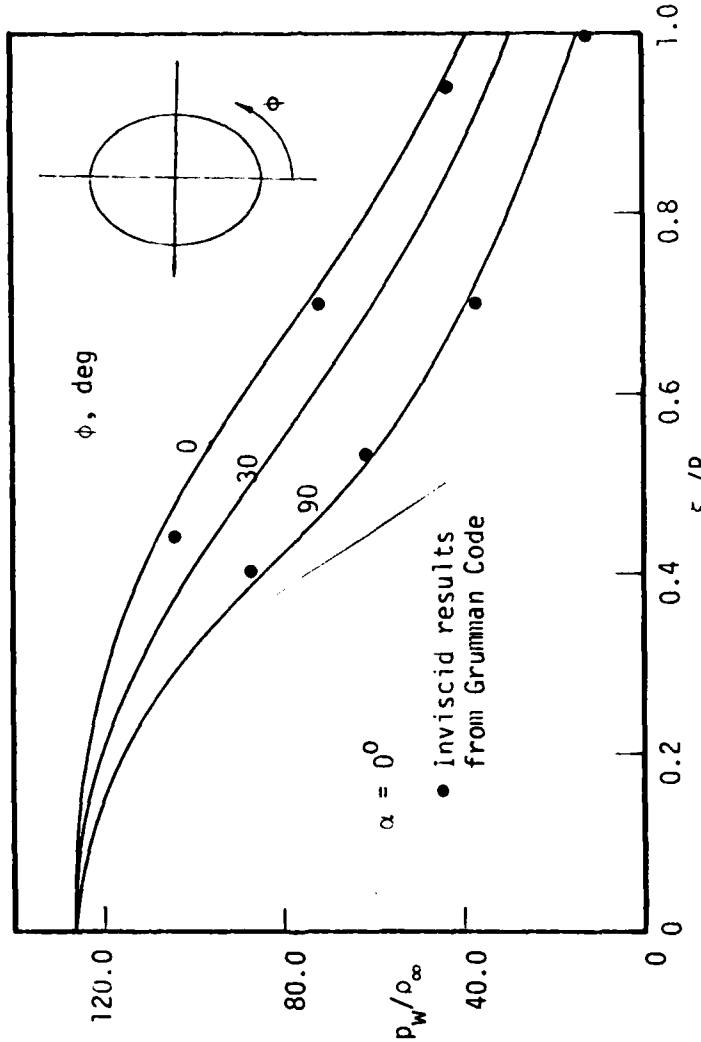

Figure 4. Surface pressure for 1:1.4 Ellipsoid

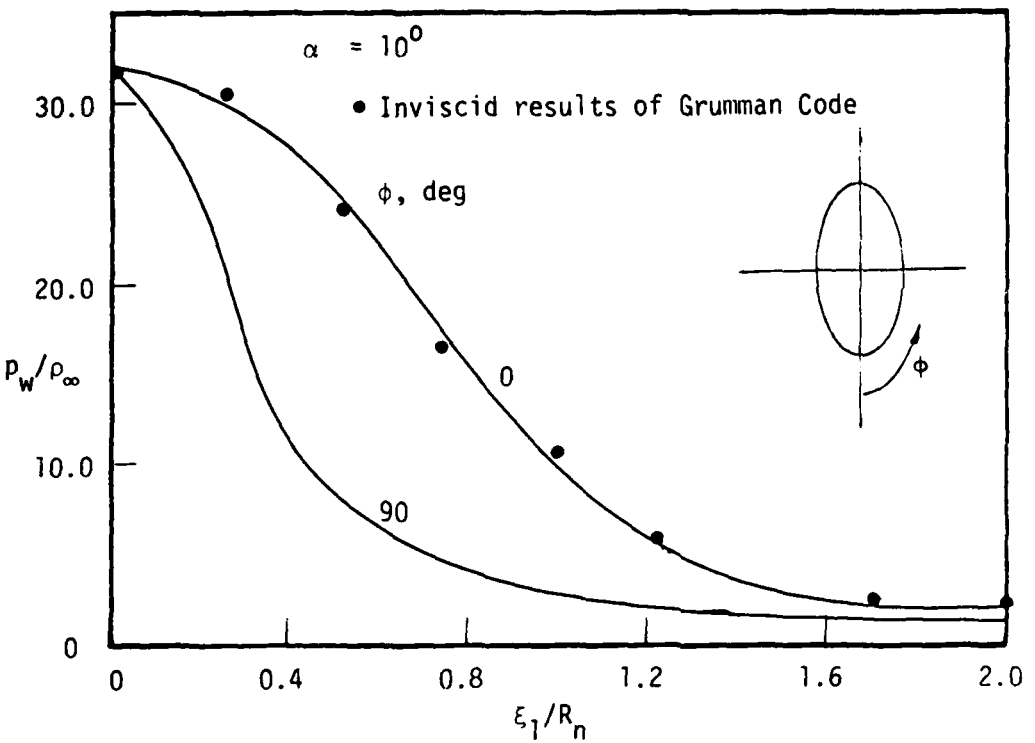

Figure 5. Surface Pressure for 1:2 Ellipsoid

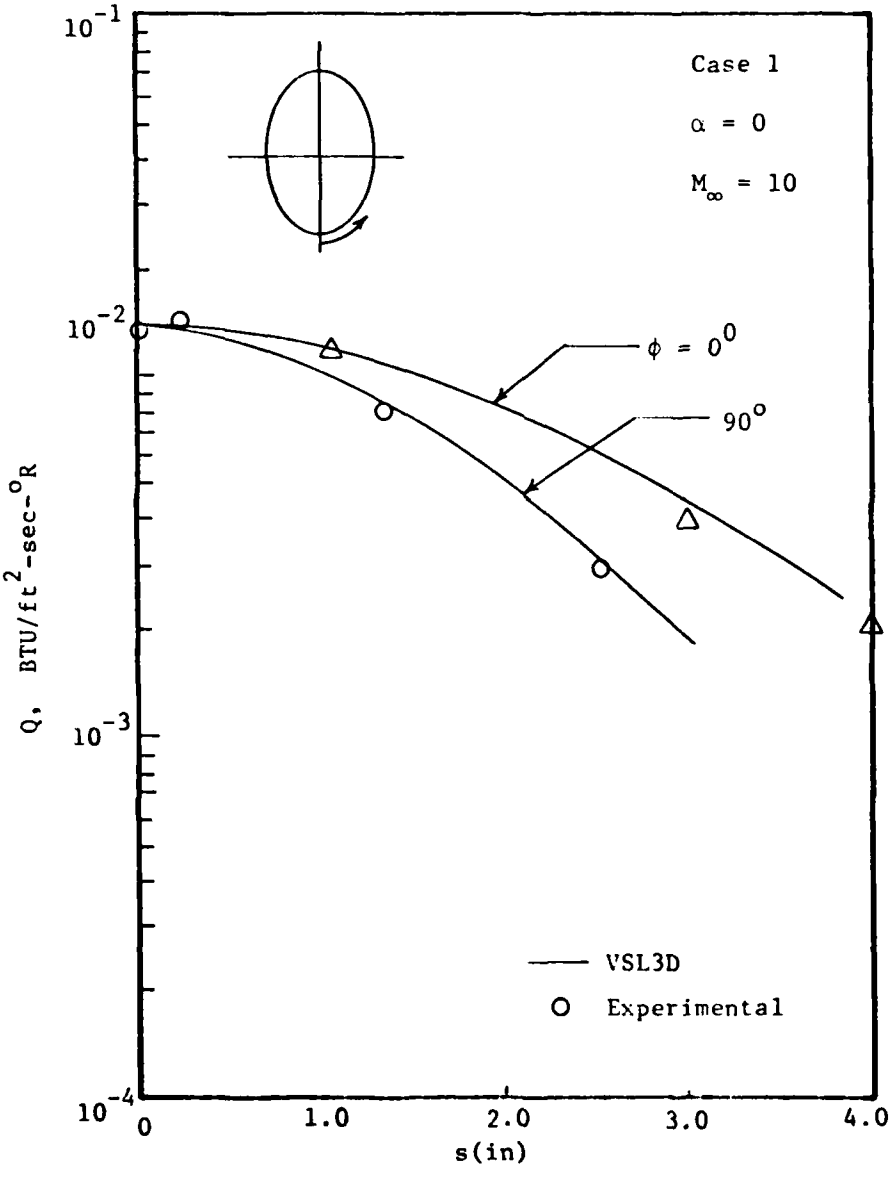

Figure 6. Convective Heat Transfer to 1:43 Ellipsoid.

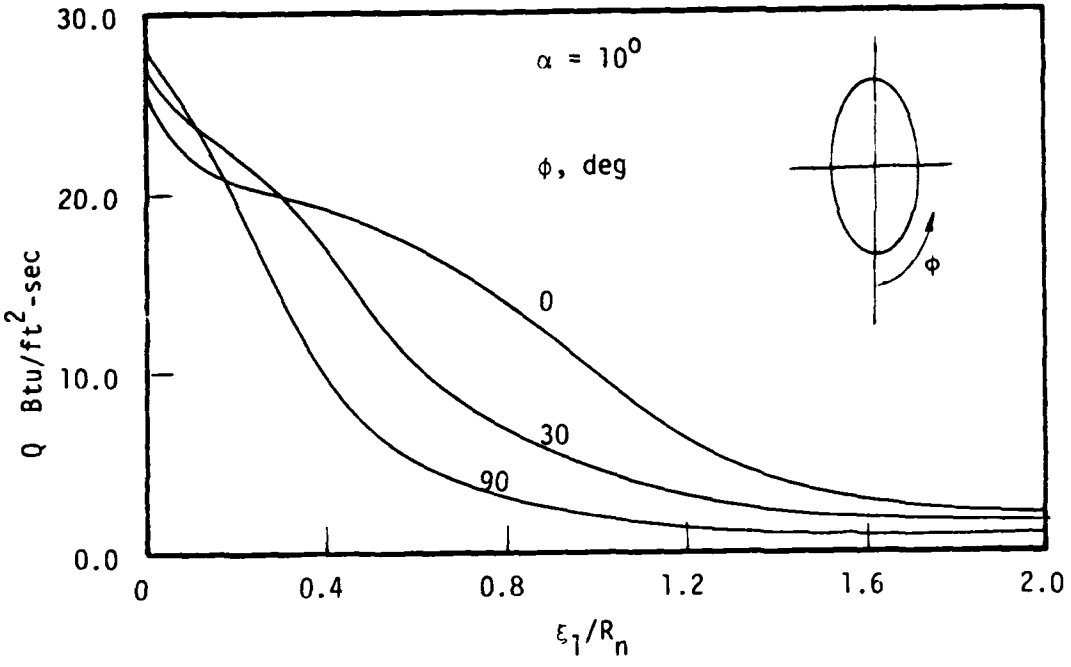

Figure 7. Convective Heat Transfer to 1:2 Ellipsoid

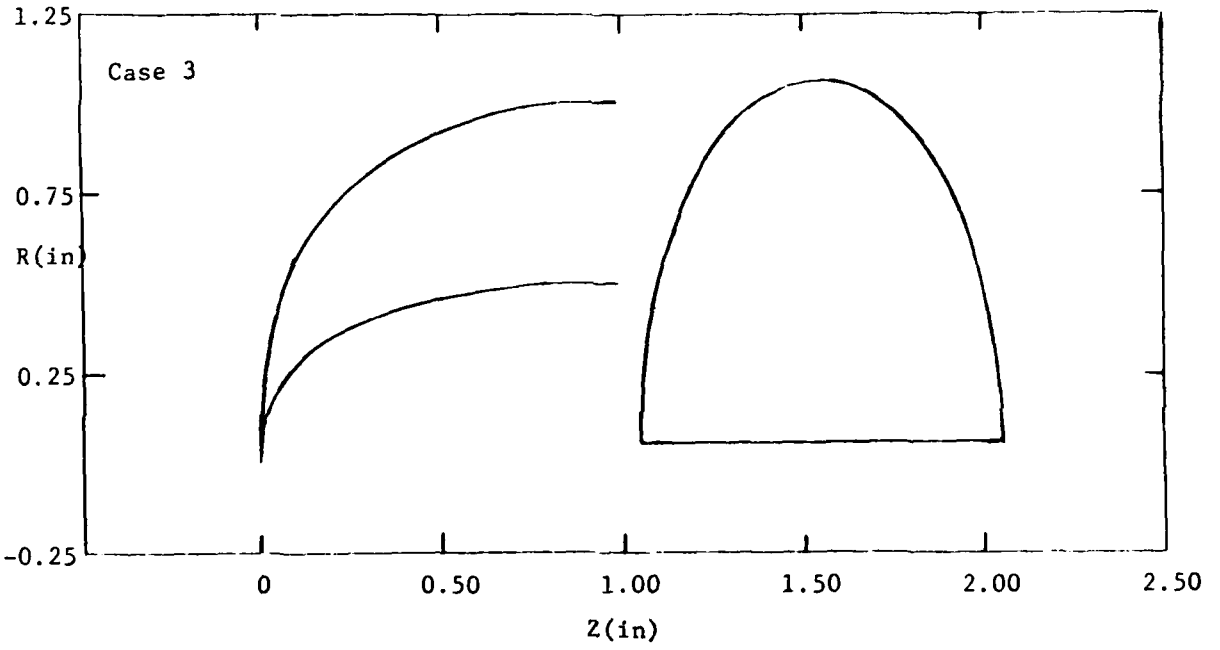

Figure 8. The Geometry of Modified 1:2 Ellipsoid.

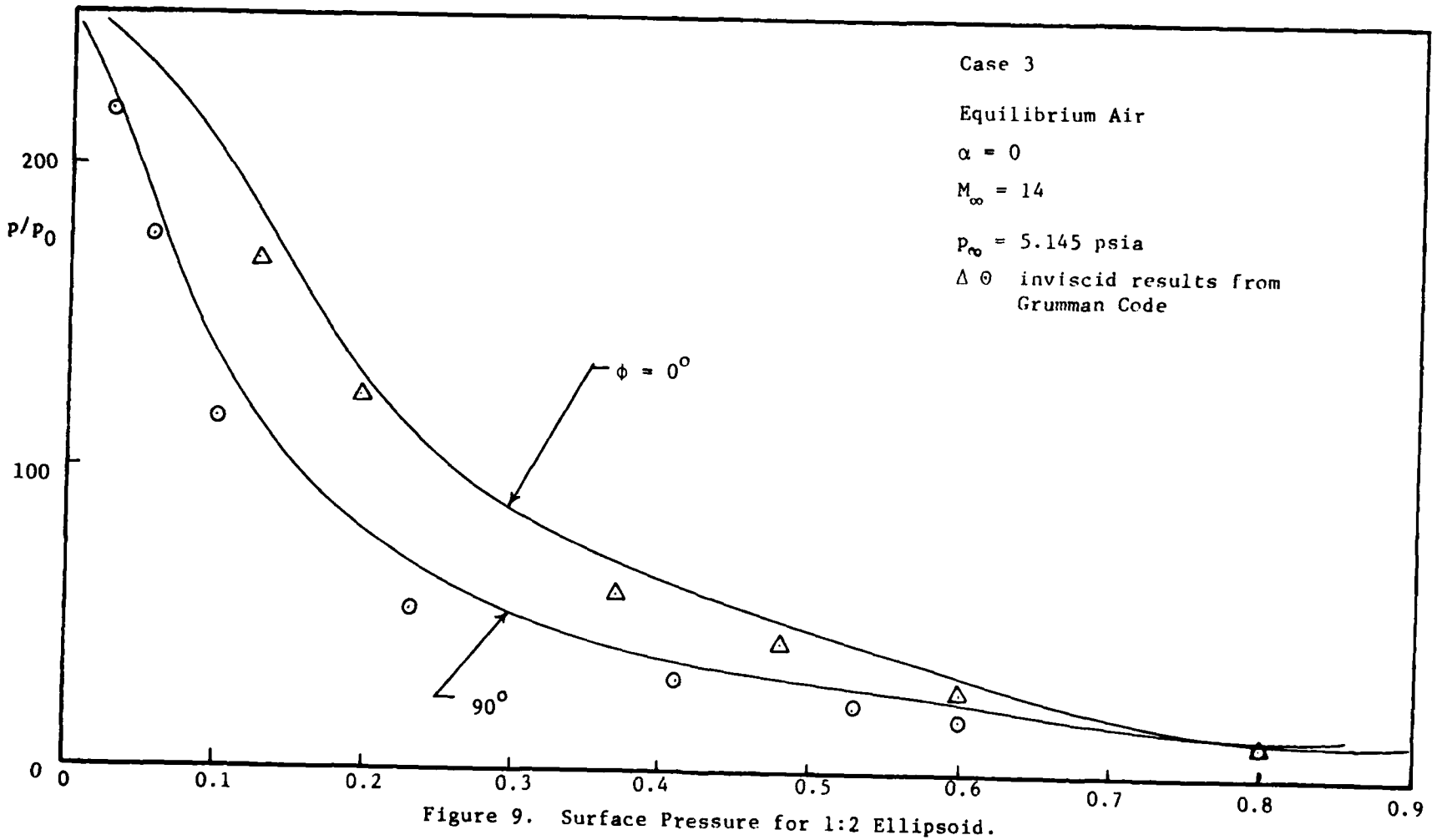

Figure 9. Surface Pressure for 1:2 Ellipsoid.

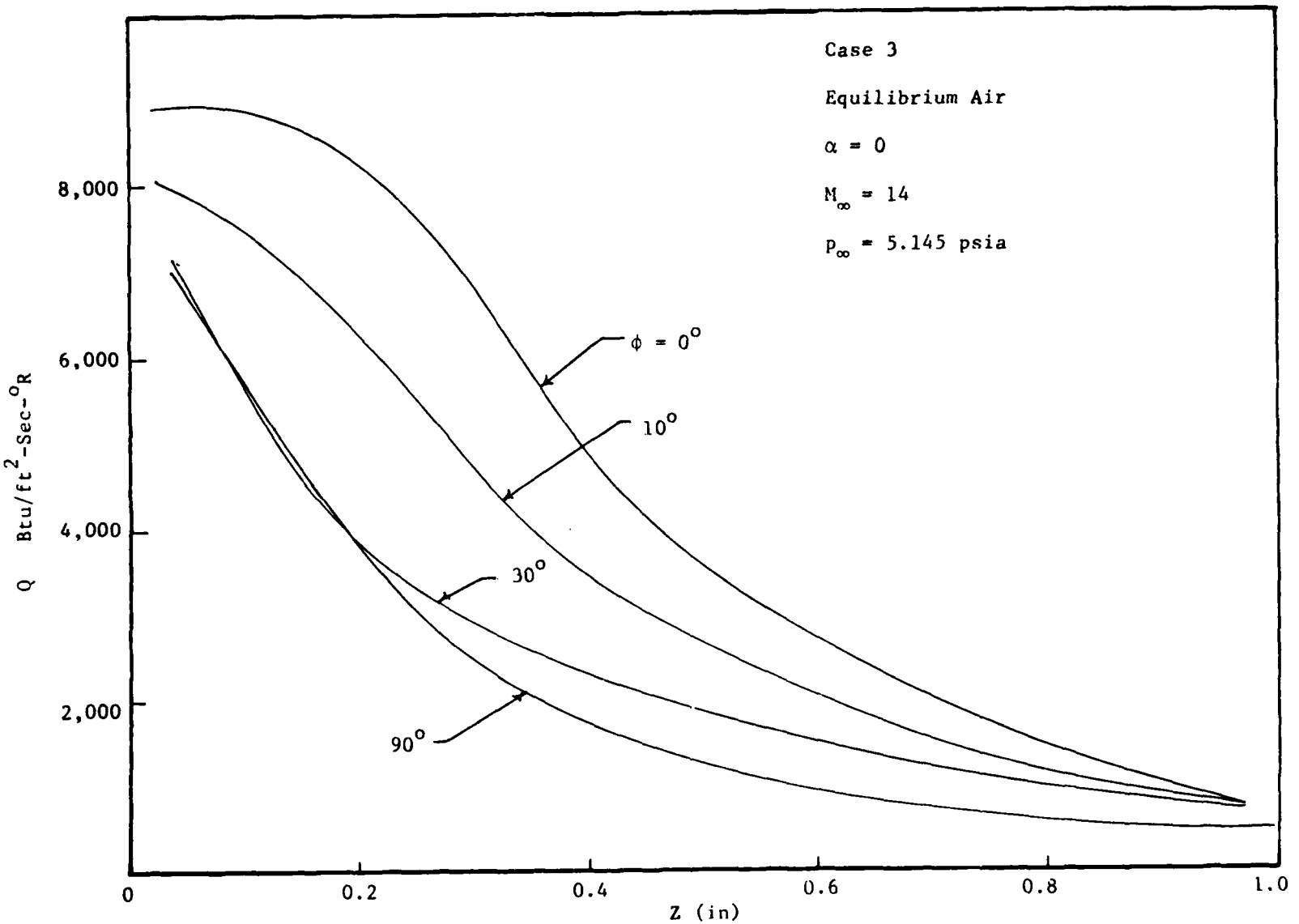

Figure 10. Convective Heat Transfer to 1:2 Ellipsoid.

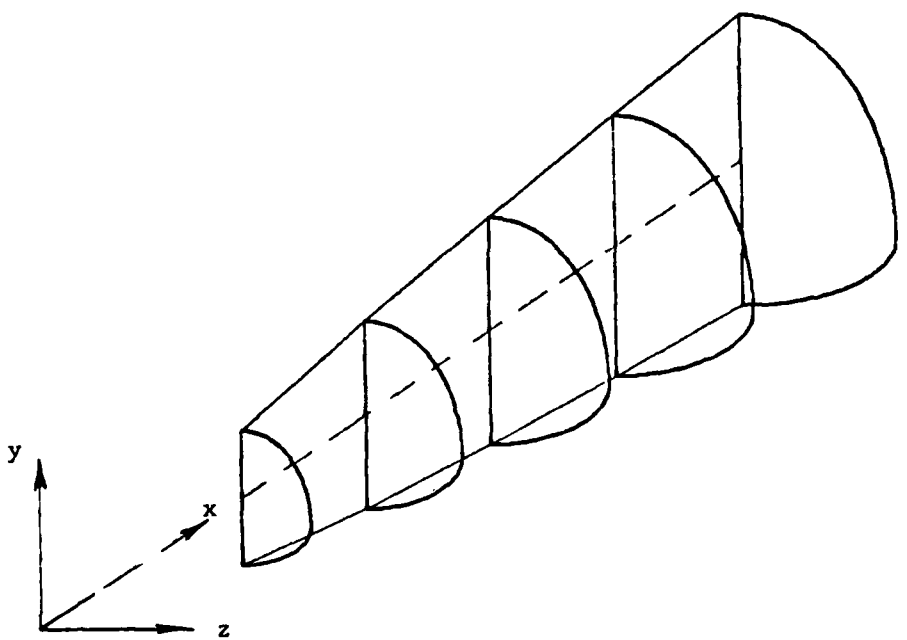

Figure 11. The Geometry of Shuttle Orbiter

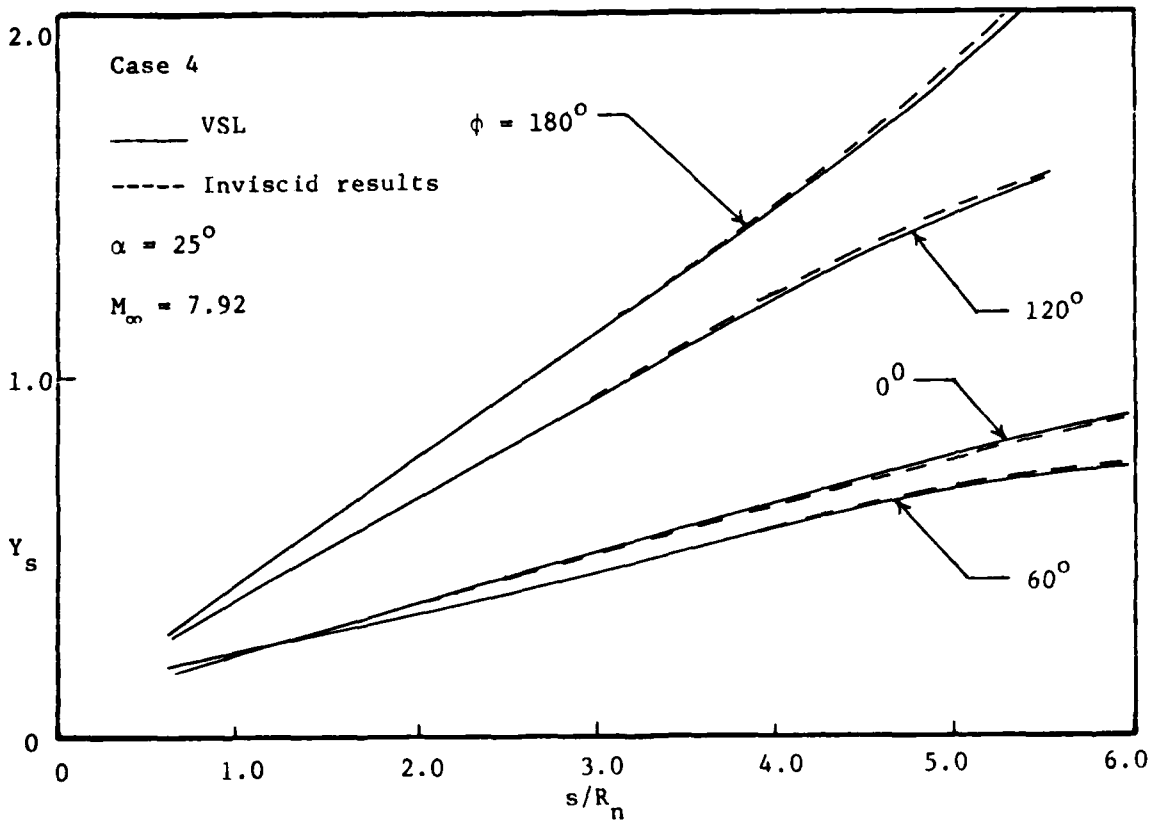

Figure 12. Shock Standoff Distance for Space Shuttle.

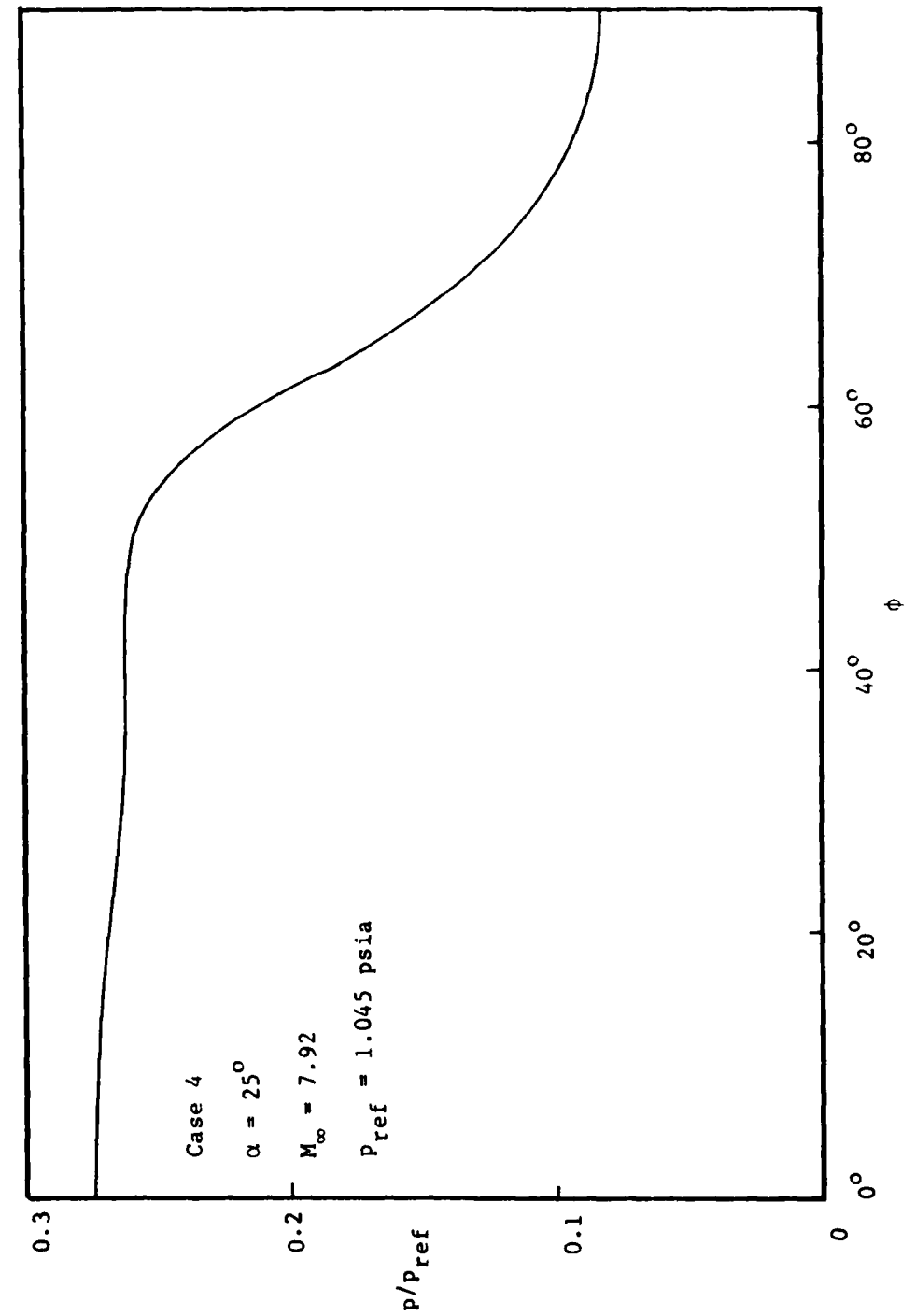

Figure 13. Space Pressure Profile for Space Shuttle at s = 5.32

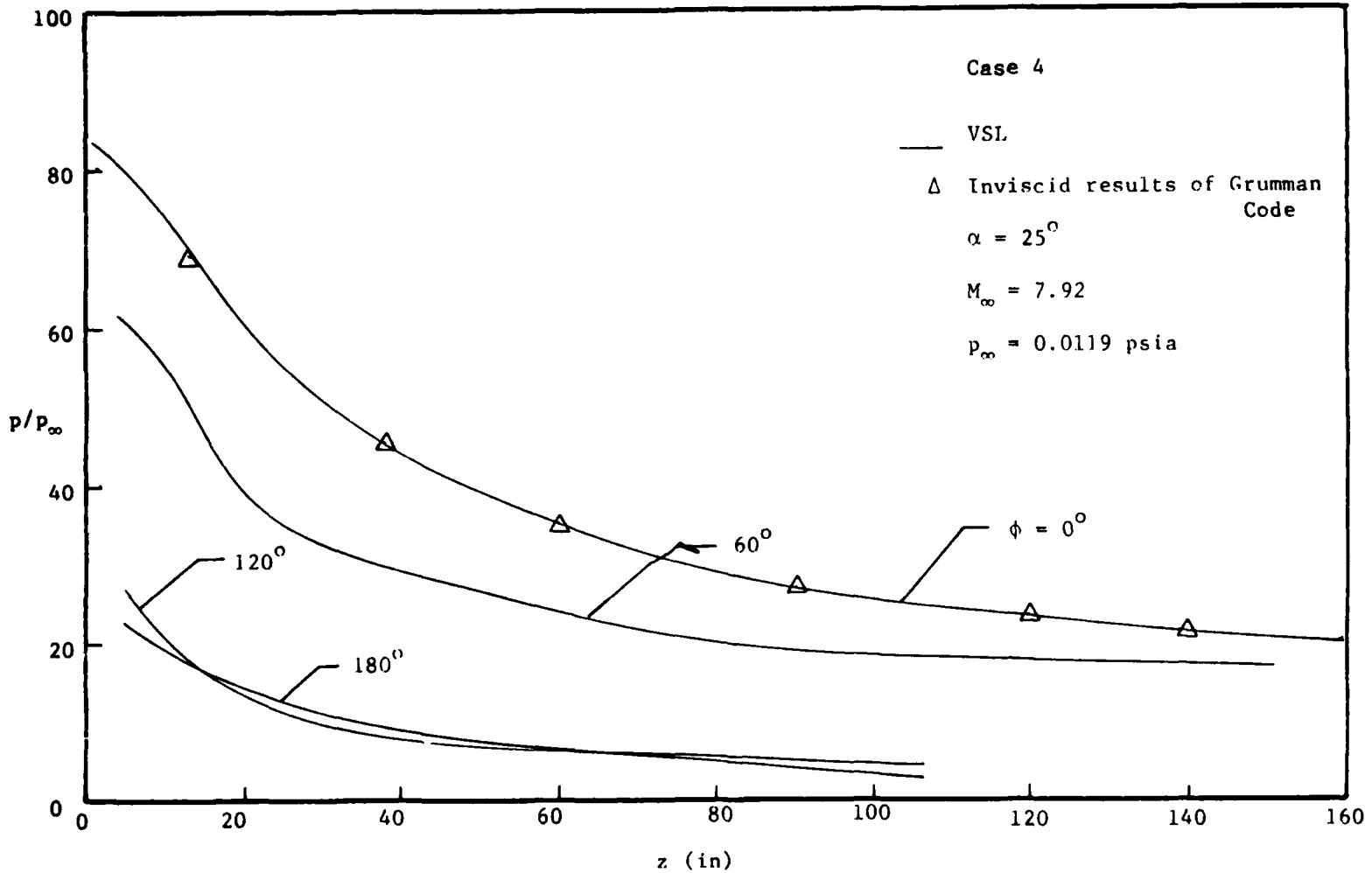

Figure 14. Space Shuttle Surface Pressure Distribution

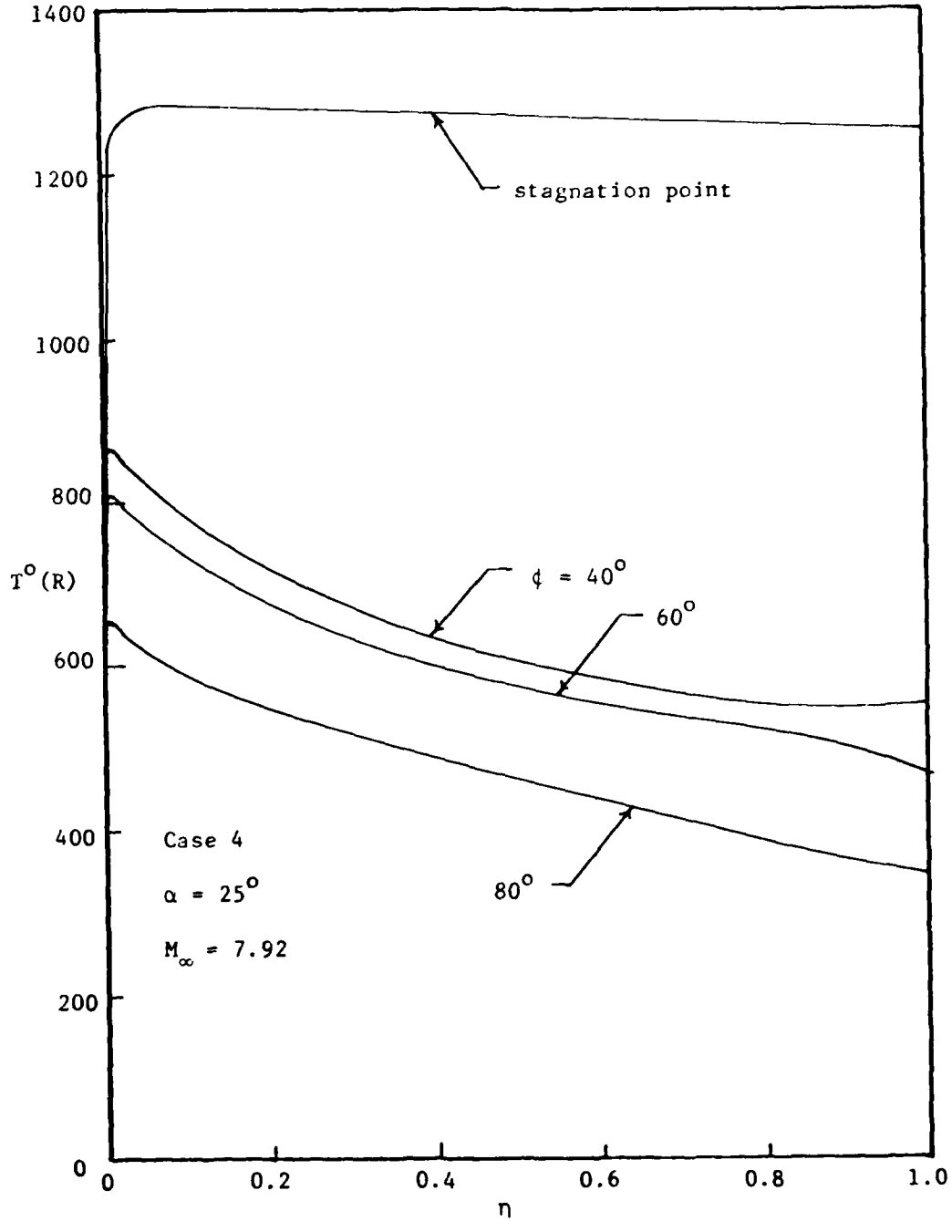

Figure 15. Space Shuttle Temperature Profile at Stagnation Point and s = 5.32

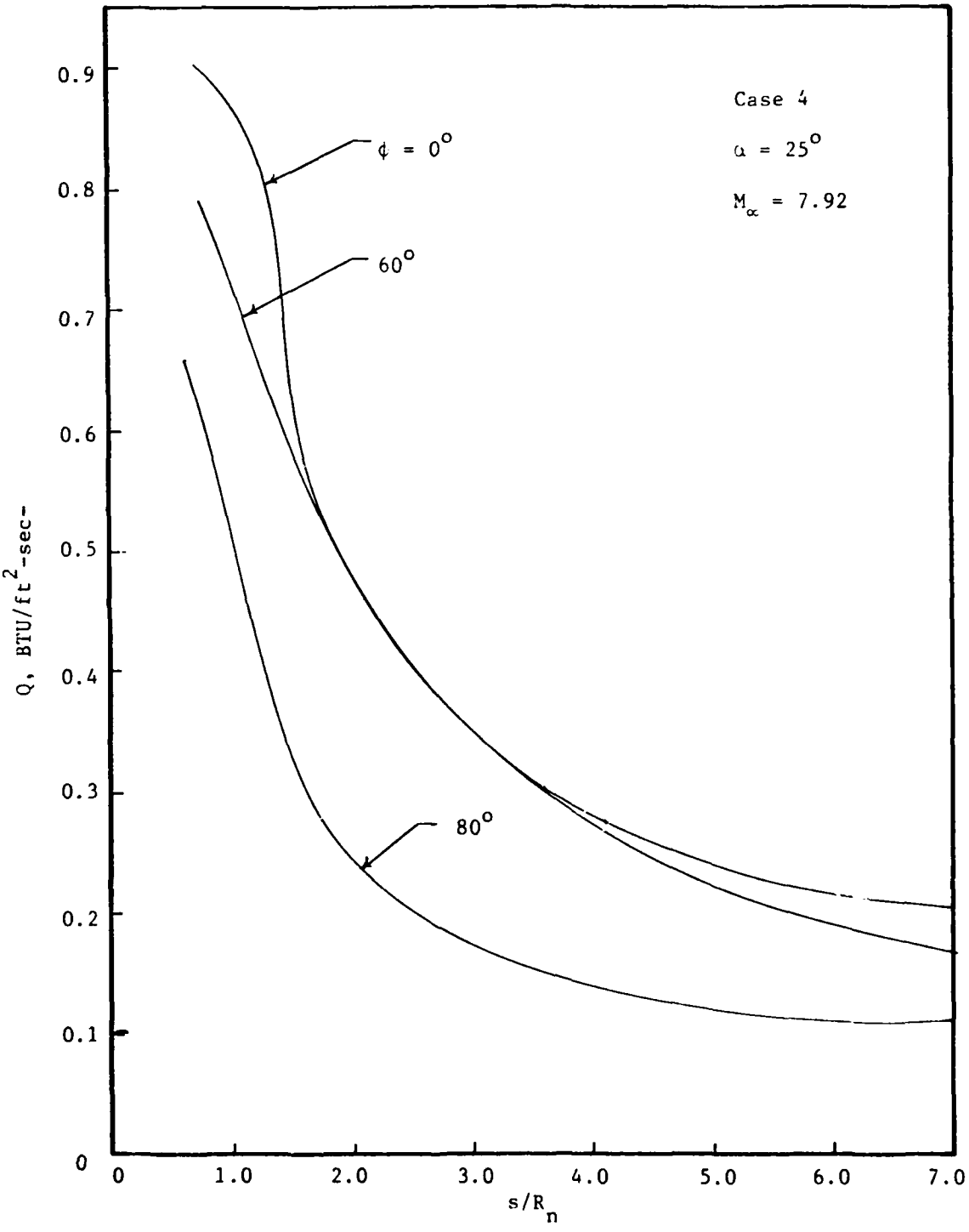

Figure 16. Convective Heat Transfer for Space Shuttle.